Thermal profile analysis of Doubly-Fed induction generator based wind power converter with air and liquid cooling methods

Zhou, Dao; Blaabjerg, Frede; Lau, Mogens; Tonnes, Michael

Published in:
Proceedings of the 15th European Conference on Power Electronics and Applications, EPE 2013

DOI (link to publication from Publisher):
10.1109/EPE.2013.6631992

Publication date:
2013

Thermal Profile Analysis of Doubly-Fed Induction Generator Based Wind Power Converter with Air and Liquid Cooling Methods

Dao Zhou[1], Frede Blaabjerg[1], Mogens Lau[2], Michael Tonnes[2]
[1] Aalborg University
Pontoppidanstraede 101, DK-9220
Aalborg, Denmark
[2] Danfoss Silicon Power GmbH
Husumer Strasse 251, D-24941
Flensburg, Germany
E-Mail: zda@et.aau.dk

Acknowledgements

The author would like to thank Klaus Olesen from Danfoss power electronics for his kind help on the liquid cooling technique.

Keywords

«Wind power converter», «Thermal profile», «Air cooling», «Liquid cooling».

Abstract

Today, wind power generation system keeps on moving from onshore to offshore and also upscaling in size. As the lifetime of the wind power converter is prolonged to 20-25 years, this paper will investigate and compare different cooling methods for power modules – the air cooling and the liquid cooling seen from a thermal profile assessment point of view. Firstly, an analytical approach from loss profile to thermal profile for the power semiconductor is proposed and verified in a 2 MW Doubly-Fed Induction Generator (DFIG) based wind turbine system. Then, the typical air cooling and liquid cooling in wind power converter are analyzed and compared in terms of the mean junction temperature and the junction temperature fluctuation. It is concluded that the liquid cooling approach has a similar junction temperature fluctuation but gives a lower mean junction temperature than the air cooling approach.

Introduction

By 2020, the European Union is ambitious to meet its climate and energy target, known as the "20-20-20" strategy [1]. The utilization of power electronic converter is nowadays playing a key role to fulfill these climate and energy targets in renewable energy conversion and industrial application (e.g. wind and solar power generation, motor drives, rail traction and hybrid-electric vehicles). Many of these converters have highly variable loads [2], [3], and more and more efforts are devoted into the reliability characteristic, in which the thermal cycling is regarded as the most significant impact among the different stressors (vibration, contaminants, humidity, etc.). It is widely accepted that the thermal profile of power semiconductor is an important indicator of the lifetime and it has an influence on the reliable operation. The power cycle number to failure is quite relevant to the junction temperature fluctuation as well as the mean junction temperature [4].

The power density is steadily being increased [5], [6] – although it has benefits in an improvement of functions, an enhanced power range and a reduced impact on volume and cost, it demand extra amount of the heat-sink for the power converter in order to extract the same dissipating energy from a smaller heat-sink size, which is potentially increasing the severity of the thermal cycling and reducing the device reliability [7]. In a full-scale power converter, the typical amount of heat that has to be transported away from the power modules may be from 50 kW to 100 kW for a 2 MW wind turbine

[8]. Because the cooling solutions take up considerable space available in a typical wind turbine nacelle, it is interesting to investigate and analyze the different cooling system, where the forced air cooling and the liquid cooling cover 95% of all power module application.

The scope of this paper is to analyze and compare the thermal profile of power modules for conditions of air cooling and liquid cooling. Firstly, an analytical approach from loss profile to thermal profile for power semiconductor is proposed and verified in a multi-MW Doubly-Fed Induction Generator (DFIG) based wind turbine system. Then, the typical approaches for air cooling and liquid cooling in wind power converter are evaluated and compared in terms of the mean junction temperature and the junction temperature swing.

Analytical approach to evaluate thermal profile

According to the basic layout of the power semiconductor module, the one-dimension thermal model is given in forms of typical power module configurations. Then, an analytical approach to evaluate the thermal profile from the power loss profile is proposed.

Power module assemblies

The layout of a typical power semiconductor module is depicted in Fig. 1. A number of power semiconductor chips – IGBTs and diodes are soldered onto the ceramic based substrates like DBC (Direct Bond Copper), which acts as an electric isolator. The DBC substrate can be either soldered onto a baseplate, or the bottom copper layer is directly mounted to a heat-sink with Thermal Interface Material (TIM) in between. The electrical connections between chips and conductor tracks on the DBC are normally realized by thick wire-bonding of pure aluminum.

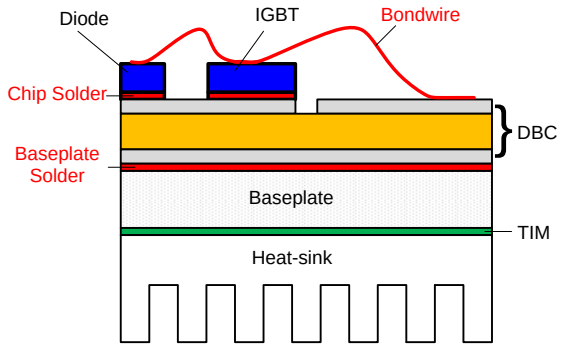

Fig. 1: Basic structure of a power semiconductor module.

Thermal model

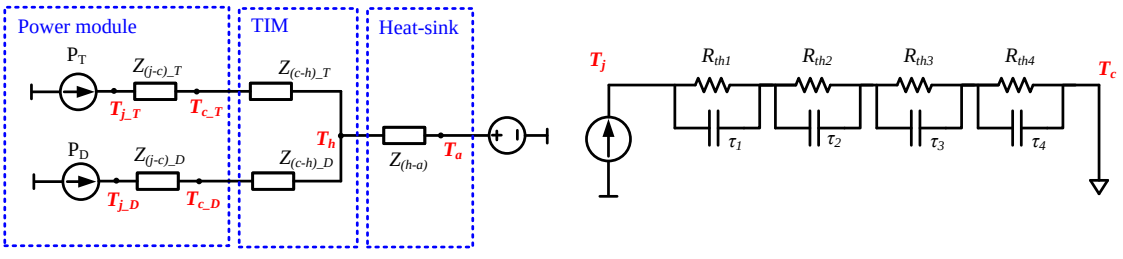

(a) (b)

Fig. 2: Thermal model of the power devices. (a) Thermal model of single IGBT and diode (from junction to ambient). (b) Equivalent Foster RC thermal network (from junction to case).

The thermal model of power devices, including the IGBT and the freewheeling diode are shown in Fig. 2(a) in forms of the power module, the thermal grease and the heat-sink. The electrical analogies representing thermal variable are used [9]-[12], in which the power dissipation in the IGBT and the

diode are expressed as the current source, the voltage source stand for the constant temperature levels, and RC elements are used to signify the thermal impedance.

The thermal impedance from junction to case is modeled as a four-layer Foster RC network as shown in Fig. 2(b), whose values are normally provided by the manufacturer's datasheet. Meanwhile, the ambient temperature is set to 50 ℃ as an indication of the worst case.

Analytical method for thermal profile

A typical thermal profile of the power semiconductor in a wind power converter contains large thermal cycles and small thermal cycles, which are driven by wind turbulence and bidirectional current within a fundamental frequency, respectively. At first glance, the lifetime and reliability issue of the wind energy generation system induced by wind turbulence is more crucial due to the larger junction temperature fluctuation of the power semiconductor. However, it is still essential to look into the influence of small thermal cycles due to their greater order of magnitude, because the loading current normally changes in several seconds, while the fundamental period of current is actually from dozens of milliseconds to hundreds of milliseconds.

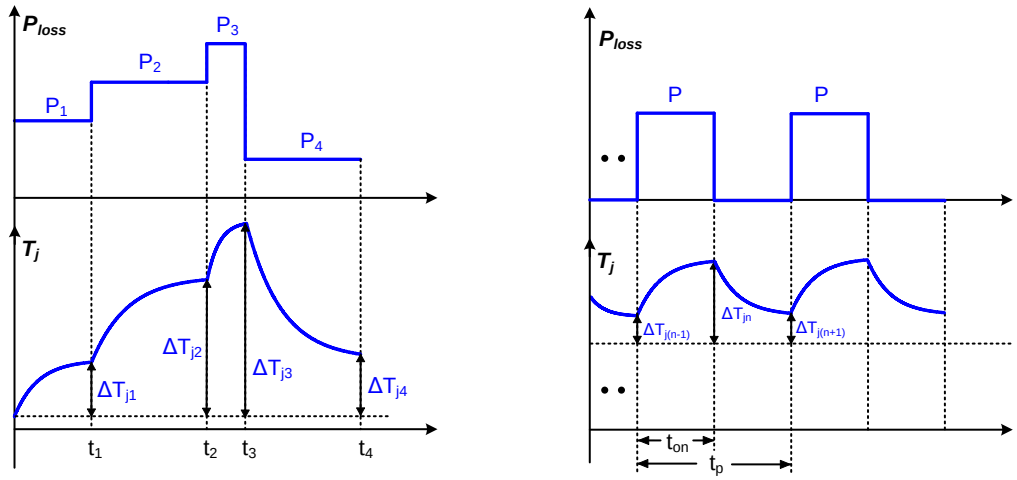

Fig. 3: Power loss profile and junction temperature profile against time. (a) Step pulse of power dissipation. (b) Periodical pulse of power dissipation.

Fig. 3(a) shows the step pulse of power loss, and according to the thermal model in Fig. 2(b), the junction temperature fluctuation ΔT_{jn} during n^{th} power loss pulse can be deduced to,

$$\Delta T_{jn} = \Delta T_{j(n-1)} \sum_{i=1}^{4} e^{-\frac{t_n - t_{n-1}}{\tau_i}} + P_n \sum_{i=1}^{4} R_{thi} \left(1 - e^{-\frac{t_n - t_{n-1}}{\tau_i}}\right) \tag{1}$$

where the first item denotes the zero-input response of the previous junction temperature fluctuation $\Delta T_{j(n-1)}$ at the moment t_{n-1}, and the second term denotes the zero-state response of the power loss P_n at the moment t_n. R_{thi} and τ_i indicate i^{th} Foster structure thermal resistance and time constant, which are both consisted with the value shown in Fig. 2(b). According to equation (1), the junction temperature swing can be easily inferred from power loss profile in time domain.

Fig. 3(b) shows the case of thermal profile in the condition of periodical pulse of power dissipation. The junction temperature fluctuation at moment t_{n-1}, t_n, and t_{n+1} can be calculated by equation (1), respectively. Since $\Delta T_{j(n+1)}$ has the same value as $\Delta T_{j(n-1)}$ at the steady-state operation, the junction temperature fluctuation and the mean junction temperature are expressed as equation (2) and (3), respectively.

$$\Delta T_j = P \sum_{i=1}^{4} R_{thi} \frac{\left(1 - e^{-\frac{t_{on}}{\tau_i}}\right)^2}{1 - e^{-\frac{t_p}{\tau_i}}} \tag{2}$$

$$T_{jm} = \sum_{i=1}^{4} R_{thi} \cdot \frac{P}{2} + T_a \tag{3}$$

where P is the peak value of periodical power pulse, t_{on} denotes the on-state time, t_p denotes the fundamental period of converter output current, and T_a denotes the ambient temperature. It is noted that t_p is twice value of t_{on}. Based on equation (2) and (3), the thermal behavior of the power device at steady-state can be analytically deduced, which avoids time-consuming simulation due to the huge difference between the switching period and the thermal time constant of the power device.

Case study in a 2 MW DFIG wind turbine system

In this section, based on the power loss profile of the back-to-back power converter in a 2 MW DFIG wind turbine system, the analytical method for power device junction temperature will be evaluated and analyzed. In order to verify the analytical estimation for thermal behavior of the power semiconductor, a comparison with the simulation results is then implemented.

Basic concept and power loss profile of DFIG system

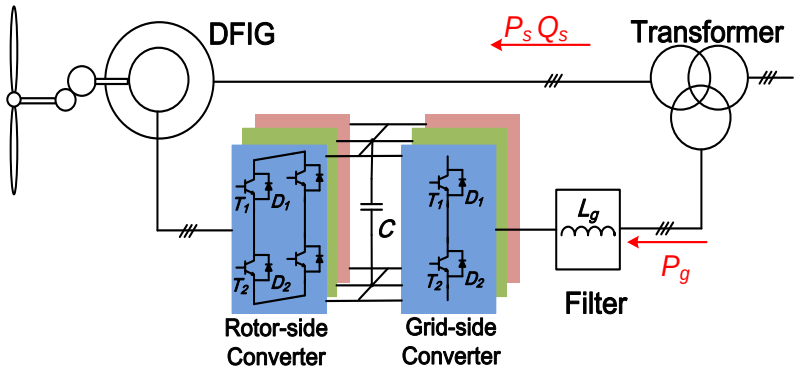

Fig. 4: Typical configuration of a DFIG wind turbine system.

Due to the extensive and well-established knowledge, as well as the simpler structure and fewer components, the two-level back-to-back voltage source converter is the most attractive solution in the commercial market of wind turbine system. A popular wind turbine configuration, normally based on a DFIG, is to employ a partial-scale power converter, as shown in Fig. 4. The function of the rotor-side converter is not only to transfer the slip active power from/to the grid, but also to provide excitation energy for the induction generator, while the grid-side converter is designed to keep the DC-link voltage fixed and supply part of the reactive power required by the grid codes. The parameters of the used induction generator and back-to-back power converter are summarized in Table I and Table II, respectively. It is noted that due to the significantly unequal current through the grid-side converter and rotor-side converter, single common low-voltage power device (1.7 kV/1 kA) and two paralleled power devices is the solution for each the grid-side converter and the rotor-side converter bridge arm for a 2 MW wind turbine system.

Table I: Parameters for a 2 MW DFIG

Rated power P_m	2 MW
Reactive power range Q_s	-570 kVar ~ +450 kVar
Rated peak stator voltage U_{sm}	563 V
Stator/rotor turns ratio k	0.369
Stator inductance L_s	2.95 mH
Rotor inductance L_r	2.97 mH
Magnetizing inductance L_m	2.91 mH

Table II: Parameters for back-to-back power converter

Rated power P_g	330 kW
Rated peak phase voltage U_{gm}	563 V
DC-link voltage U_{dc}	1050 V
Filter inductance L_g	0.5 mH
RSC and GSC switching frequency f_s	2 kHz
Power device in each grid-side converter cell	1.7 kV/1 kA
Power device in each rotor-side converter cell	1.7 kV/1 kA // 1.7 kV/1 kA

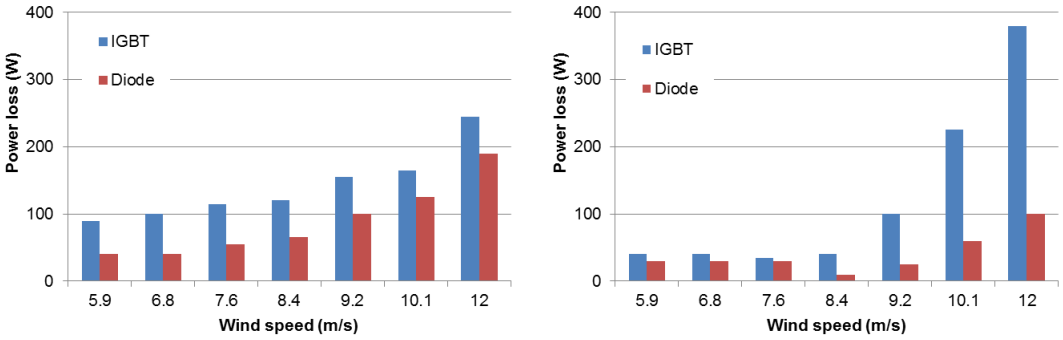

(a) (b)

Fig. 5: Power loss profile of each power device for the back-to-back power converter in the DFIG system. (a) Rotor-side converter. (b) Grid-side converter.

In order to investigate the loss behavior in different operation modes, several wind speeds are chosen in the DFIG system. It is worth to mention that the wind speed at 8.4 m/s is regarded as the synchronous operation point of the DFIG system. Based on the loss energy curves provided by the manufacturer, the accumulated power dissipation in every switching cycle can be obtained within one fundamental frequency. Simulations have been realized by the PLECS block in Simulink [13]. The loss distribution of the IGBT and diode in the rotor-side converter at different wind speeds is shown in Fig. 5(a). In order to avoid an extremely unbalanced power device loading at synchronous operation point, a small turbine speed hysteresis is introduced for the minimum rotor frequency 1 Hz [14]. The power loss in the grid-side converter at different wind speeds in shown in Fig. 5(b). The lowest power loss appears in synchronous operation due to the fact that no active power flow exist and only the switching ripple current affects, while the highest power loss emerges above rated wind speed.

Liquid cooling techniques for power module

Liquid cooling solutions for the power module are mainly divided into indirect cooling and direct cooling. Indirect cooling means that the power module is assembled on a closed cooler through a thin layer of thermal interface material (e.g. cold plate). On the other hand, direct cooling means that the coolant is in direct contact with the surface to be cooled, which is commonly done by pin fin designs or a paralleled liquid cooling of the whole base plate surface area. Direct liquid cooling eliminates the layer of thermal interface material that is traditionally needed between the backside of the power module and cold plate. As the thermal grease accounts for up to 50% of the thermal resistance from the junction to ambient [15], this elimination results in an improved thermal environment for the power module.

Thermal profile estimation by typical liquid cooling

Due to different materials as well as their unequal thermal expansion coefficient, the thermal impedance normally includes the junction to case, the case to heat-sink and the heat-sink to ambient. The thermal impedance from the junction to case is usually tested by the manufacturer, and their

values is given in terms of multi-layer Foster RC network, which is the curve fitting value and has no real physical meaning. Moreover, in order to evaluate the correct junction temperature, the thermal impedance from case to heat-sink and the heat-sink to ambient are essential to take into account, as even with the highest quality standards for application of thermal interface material, the thermal resistance of interface material is in the same magnitude as the module itself [16]. However, the series connection of Foster model will inevitably introduce significant errors, so the best method to estimate the junction temperature of the power semiconductor is to use the thermal impedance directly from the junction to ambient, and the thermal impedance of a direct liquid cooling per power device is illustrated in Fig. 6. It can be seen that the maximum time constant for the thermal network is several seconds. Furthermore, the diode has poorer dynamical thermal impedance than the transistor in the entire time domain and also it has a higher steady-state thermal resistance.

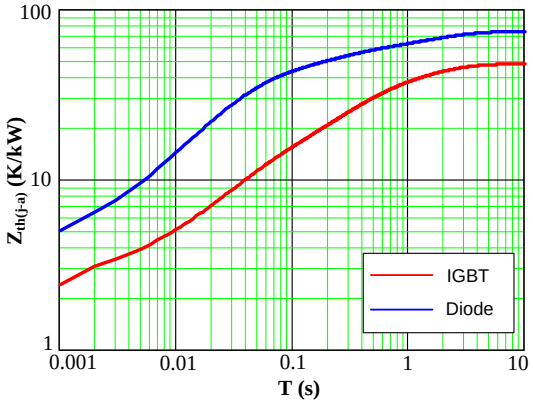

Fig. 6: Thermal impedance from junction to heat-sink of a typical liquid cooling.

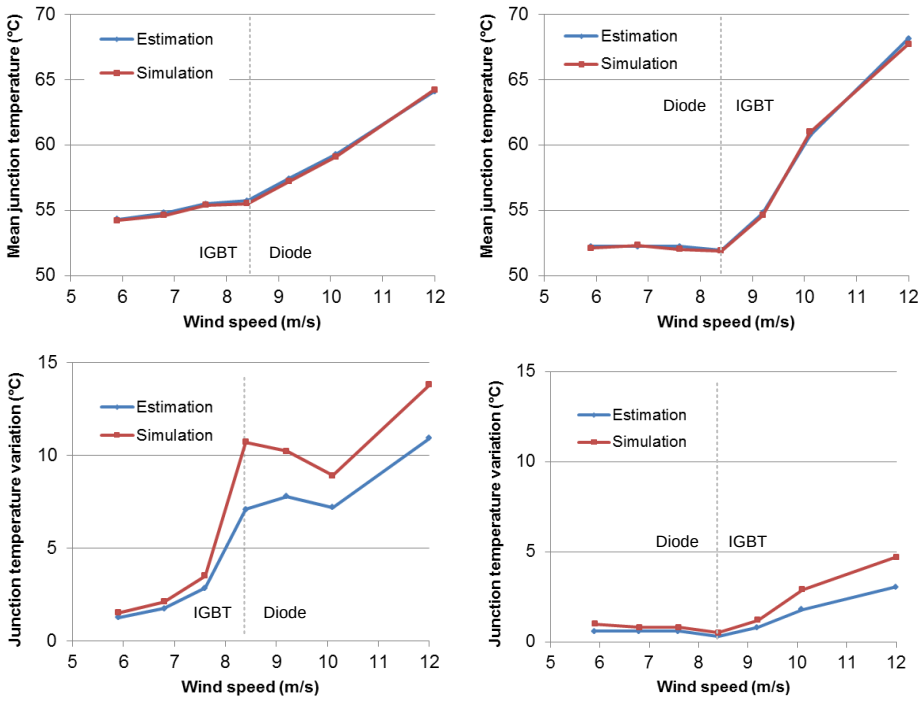

(a) (b)

Fig. 7: Analytical estimation vs. simulation results of the junction temperature profile in device-chips. (a) Rotor-side converter. (b) Grid-side converter. (Note: "IGBT" indicates the operating area where the IGBT is more loaded, and "Diode" indicates the operating area where the diode is more loaded).

In order to evaluate the thermal performance of the power device of the back-to-back power converter at different wind speeds, along with the power loss profile shown in Fig. (5), the junction temperature

fluctuation and the mean junction temperature can be calculated by equation (2) and (3), respectively, where for simplicity the instant sinusoidal power loss is regarded as step-changing power loss. As a consequence, a comparison of the junction temperature profile in the power semiconductors between analytical method and simulation is shown in Fig. 7, where the most stressed power devices of the rotor-side converter and the grid-side converter are extracted in Fig. 7(a) and Fig. 7(b), respectively. It is evident that the mean junction temperature is well predicted by the proposed method. However, the estimation results will have a lower junction temperature fluctuation due to the fact that the power dissipation is regarded as the step source instead of the sinusoidal. Moreover, for the rotor-side converter, the hottest device moves from the IGBT to the diode, if the DFIG operation change from sub-synchronous mode to super-synchronous mode, while for the grid-side converter, the IGBT has a higher mean junction temperature and the junction temperature fluctuation in case of the super-synchronous operation mode.

Thermal profile comparison between air cooling and liquid cooling

Nowadays air cooling and liquid cooling are the popular two cooling techniques for power modules. Thermal impedance for typical air and liquid cooling is first to be evaluated and analyzed, then improved thermal model for these two approaches are described, respectively. Thermal behavior between air cooling and liquid cooling is finally compared.

Analysis of typical air cooling and liquid cooling

Fig. 8(a) shows the typical heat-sink thermal impedance for these cooling approaches from Semikron [4]. It can be seen that the time constant from the heat-sink to ambient (dozens of seconds to hundreds of seconds) is much longer than that from the junction to case (dozens of milliseconds to several seconds). Regarding the mean junction temperature, it is noted that the steady-state thermal resistance of air cooling is three times larger than the liquid cooling.

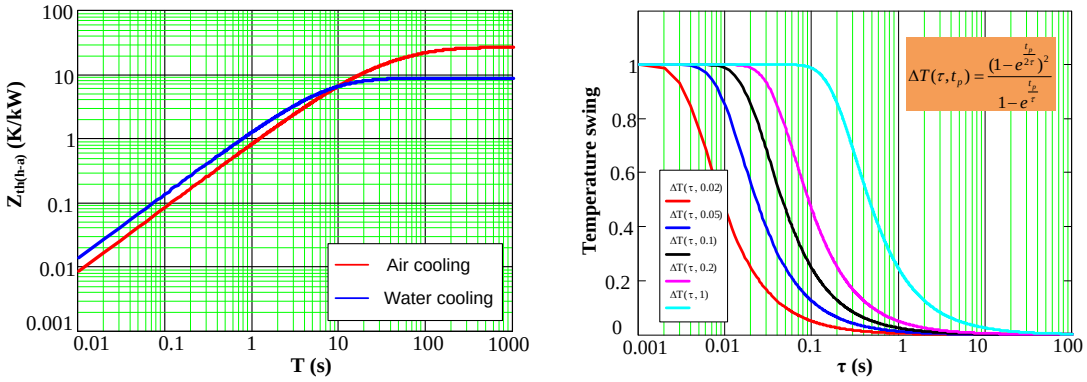

Fig. 8: Thermal impedance curve from Semikron [4]. (a) Dynamic thermal impedance of air and liquid cooling from heat-sink to ambient (Note: air flow=610 m^3/h, T_a=25 ℃, 500m above sea level; liquid flow=15 L/min, T_{fluid}=40 ℃, water/glycol ratio=50%/50%). (b) Temperature swing dependence of thermal time constant and fundamental frequency.

In order to evaluate the influence of the cooling method on the junction temperature fluctuation, the relationship between the junction temperature swing and the time constant of the thermal impedance at all possible fundamental frequencies of the output current (from 20 milliseconds to 1 second) is shown in Fig. 8(b). It can be seen that the temperature swing can almost be ignored if the thermal time constant is above 10 seconds.

Practical thermal model

For the air cooling, the datasheet of the power module does not mention any thermal information from the heat-sink to ambient because of the different applications. Assuming that typical liquid cooling and

air cooling have the same thermal resistance from the case to heat-sink, along with that the thermal impedance from the junction to case is always provided by the manufacturer, the thermal impedance from heat-sink to ambient can be inferred. Moreover, as mentioned above, the thermal impedance from the heat-sink to ambient for typical air cooling is three times larger than the liquid cooling. The parameters of the whole thermal chain for liquid cooling and air cooling are summarized in Table III.

Table III: Parameters of the whole thermal chain for liquid cooling and air cooling

		$R_{th(j\_c)}$	$R_{th(c\_h)}$	$R_{th(h\_a)}$
IGBT [K/kW]	Liquid cooling	23	5	20
	Air cooling	23	5	60
Diode [K/kW]	Liquid cooling	45	11	20
	Air cooling	45	11	60

With the air cooling method, the calculated heat-sink temperature rise falsifies the junction temperature only to a very small degree, because the time constant of heat-sink (from dozens of seconds to several hundreds of seconds) is far above of the value for power module itself (several seconds). Therefore, since the junction temperature fluctuation mainly depends on the thermal impedance from the junction to case, the improved thermal model is shown in Fig. 9(a), where the steady-state temperature rise introduced by thermal grease and air cooling is depicted as the controlled temperature source.

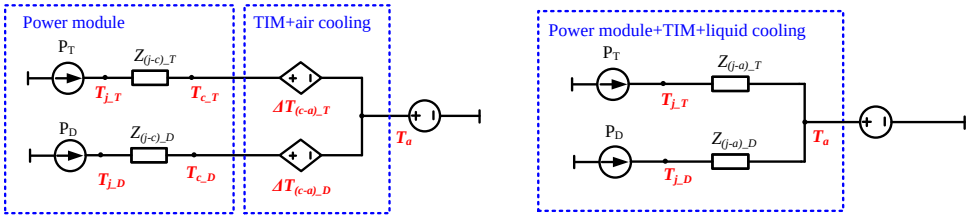

Fig. 9: Practical thermal model of the power devices. (a) Air cooling. (b) Liquid cooling.

On the other hand, the error induced by the liquid cooling is critical, since it have comparably low thermal capacities, i.e. corresponding low time constant. As a consequence, the whole thermal impedance from junction to ambient is shown in Fig. 9(b).

Thermal behavior comparison of air cooling and liquid cooling

With the aid of practical thermal model for air cooling and liquid cooling, the analytical prediction for the thermal performance of the power device can be implemented. Therefore, a comparison of the thermal cycling profile in terms of the mean junction temperature and the junction temperature fluctuation is shown in Fig. 10. For the rotor-side converter, the hottest device moves from the IGBT to the diode, if the DFIG changes from sub-synchronous operation mode to super-synchronous operation mode, while for the grid-side converter, the IGBT has a higher mean junction temperature and the junction temperature fluctuation in the case of the super-synchronous operation mode.

For the mean junction temperature, the liquid cooling has a better performance during the whole wind speed range due to its lower steady-state thermal impedance from the heat-sink to ambient. Moreover, it can be seen that, for the rotor-side converter, the mean junction temperature increases with the higher wind speed, while for the grid-side converter, the mean junction temperature will reach a minimum value at synchronous operation point. For the junction temperature fluctuation, the difference between both cooling methods becomes little.

Conclusion

In this paper, an analytical approach from loss profile to thermal profile for power semiconductor is proposed and verified in a 2 MW DFIG based wind turbine system. Moreover, the air cooling and the

liquid cooling used in wind power converter are analyzed and compared. It is demonstrated that the liquid cooling approach has a similar junction temperature fluctuation but gives a lower mean junction temperature than the air cooling.

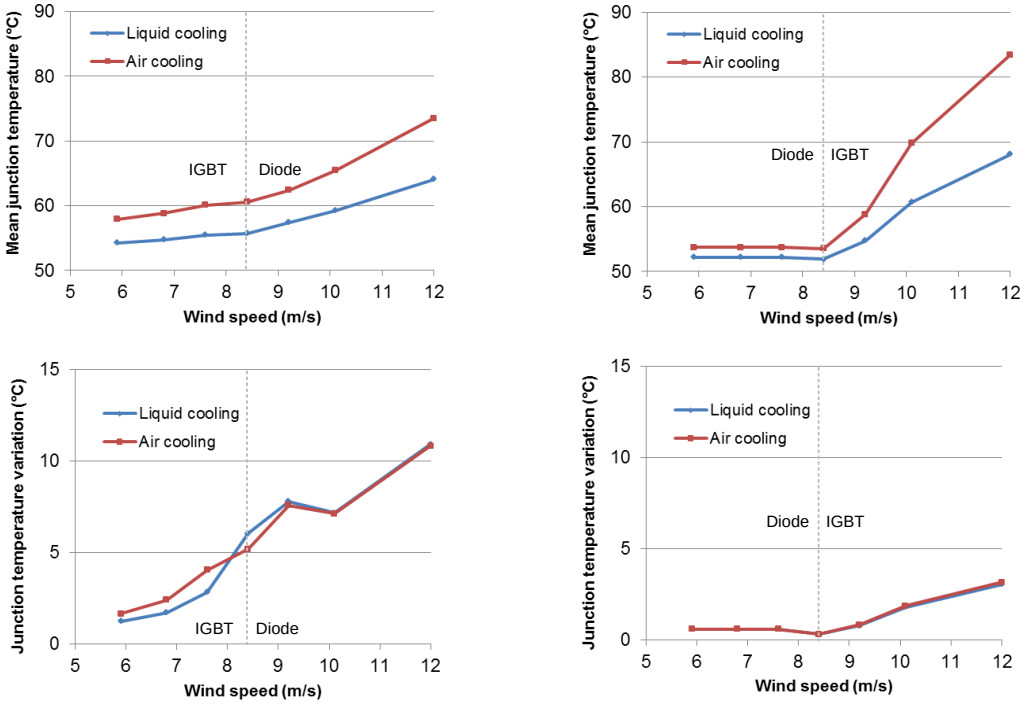

Fig. 10: Thermal profile comparison between air cooling and liquid cooling. (a) Rotor-side converter. (b) Grid-side converter. (Note: "IGBT" indicates the operating area where the IGBT is more loaded, and "Diode" indicates the operating area where the diode is more loaded).

References

[1] The EU climate and energy package. (Available: http://ec.europa.eu/clima/policies/package/index_en.htm)

[2] ZVEL, Handbook for robustness validation of automotive electrical/electronic modules, Jun. 2008.

[3] F. Blaabjerg, Z. Chen, S. B. Kjaer, "Power electronics as efficient interface in dispersed power generation systems," *IEEE Trans. on Power Electronics*, vol. 19, no. 5, pp. 1184- 1194, Sep. 2004.

[4] A. Wintrich, U. Nicolai, W. Tursky, T. Reimann, "Application manual power semiconductors," Semikron international GmbH, Nuremburg, 2011.

[5] J. Kolar, J. Biela, S. Waffler, T. Friedli, U. Badstuebner, "Performance trends and limitations of power electronic systems," *in Proc.of Integr. Power Electron. Syst. Rec*., pp. 17–36, 2010.

[6] Y. Song, B. Wang, "Survey on reliability of power electronic systems," *IEEE Trans. on Power Electronics*, vol. 28, no. 1, pp. 591-604, Jan. 2013.

[7] A. Bryant, N. Parker-Allotey, D. Hamilton, I. Swan, P. Mawby, T. Ueta, T. Nishijima, K. Hamada, "A fast loss and temperature simulation method for power converters, part I: eletrothermal modeling and validation", *IEEE Trans. on Power Electronics*, vol. 27, no.1, pp. 248-257, Jan. 2012.

[8] Q. Gao, C. Liu, B. Xie, X. Cai, "Evaluation of the mainstream wind turbine concepts considering their reliabilities," *IET on Renewable Power Generation*, vol. 6, no. 5, pp. 348-357, Sep. 2012.

[9] K. Ma, F. Blaabjerg, "Multilevel converters for 10 MW wind turbines," *in Proc. of EPE 2011*, pp. 1-10, 2011.

[10] D. Zhou, F. Blaabjerg, M. Lau, M. Tonnes, "Thermal cycling overview of multi-MW two-level wind power converter at full grid codes operation," *IEEJ Journal of Industry Applications*, to be published.

[11] D. Zhou, F. Blaabjerg, M. Lau, M. Tonnes, "Thermal behavior optimization in multi-MW wind power converter by reactive power circulation," *IEEE Trans. on Industry Applications*, to be published.

[12] H. Wang, K. Ma, F. Blaabjerg, "Design for reliability of power electronic systems," *in Proc. of IECON 2012*, pp. 33-44, 2012.
[13] User manual of PLECS blockset version 3.2.7 March 2011. (Available: http://www.plexim.com/files/plecsmanual.pdf).
[14] J. Jung, W. Hofmann, "Investigation of thermal stress in rotor of doubly-fed induction generator at synchronous operating point," *in Proc. of EWEC 2010*, pp. 1-10, 2010.
[15] K. Olesen, F. Osterwald, M. Tonnes, R. Drabek, R. Eisele, "Designing for reliability, liquid cooled power stack for the wind industry," in Proc. of IEMDC 2011, pp. 896-901, 2011.
[16] R. Schnell, M. Bayer, S. Geissmann, "Thermal design and temperature ratings of IGBT modules," ABB Application Note, 5SYA 2093-00, 2011.